ELSEVIER

NeuroImage

www.elsevier.com/locate/ynimg
NeuroImage 39 (2008) 223–230

Statistical mapping of sound-evoked activity in the mouse auditory midbrain using Mn-enhanced MRI

Xin Yu,[a,b,d] Jing Zou,[e] James S. Babb,[b] Glyn Johnson,[b] Dan H. Sanes,[f] and Daniel H. Turnbull[a,b,c,d,*]

[a]*Skirball Institute of Biomolecular Medicine, New York University School of Medicine, USA*
[b]*Department of Radiology, New York University School of Medicine, USA*
[c]*Department of Pathology, New York University School of Medicine, USA*
[d]*Graduate Program in Neuroscience and Physiology, New York University School of Medicine, USA*
[e]*Center for Computation and Mathematical Modeling, University of Maryland, College Park, USA*
[f]*Center for Neural Science, New York University, USA*

Received 16 May 2007; revised 25 July 2007; accepted 10 August 2007
Available online 29 August 2007

Manganese-enhanced MRI (MEMRI) has been developed to image brain activity in small animals, including normal and genetically modified mice. Here, we report the use of a MEMRI-based statistical parametric mapping method to analyze sound-evoked activity in the mouse auditory midbrain, the inferior colliculus (IC). Acoustic stimuli with defined frequency and amplitude components were shown to activate and enhance neuronal ensembles in the IC. These IC activity patterns were analyzed quantitatively using voxel-based statistical comparisons between groups of mice with or without sound stimulation. Repetitive 40-kHz pure tone stimulation significantly enhanced ventral IC regions, which was confirmed in the statistical maps showing active regions whose volumes increased in direct proportion to the amplitude of the sound stimuli (65 dB, 77 dB, and 89 dB peak sound pressure level). The peak values of the activity-dependent MEMRI signal enhancement also increased from 7% to 20% for the sound amplitudes employed. These results demonstrate that MEMRI statistical mapping can be used to analyze both the 3D spatial patterns and the magnitude of activity evoked by sound stimuli carrying different energy. This represents a significant advance in the development of MEMRI for quantitative and unbiased analysis of brain function in the deep brain nuclei of mice.

Introduction

Functional magnetic resonance imaging (fMRI), based on blood oxygen level dependent (BOLD) contrast, provides an effective and increasingly applied method for functional neuroimaging in humans and primates (Ogawa et al., 1990; Bandettini et al., 1992; Ogawa et al., 1993). With a major focus of neurobiology research on the genetic and molecular mechanisms underlying brain function, the mouse has become the preferred mammalian organism for many studies of brain development and disease, utilizing an array of genetic-engineering methods to generate numerous mouse models. A major challenge has been the implementation of fMRI methods with sufficient spatial resolution for analysis of the mouse brain. These challenges led us to investigate alternative MRI methods for assessing brain function and neural activity in mice.

Previously, we developed a 3D Mn-enhanced MRI (MEMRI) method for mapping sound-evoked activity in the mouse brain (Yu et al., 2005), and recently showed the utility of MEMRI for analyzing developmental plasticity in tonotopic maps of the mouse auditory midbrain (Yu et al., 2007). In this approach, neural activity was imaged retrospectively, after the accumulation of paramagnetic Mn ions within synaptically activated neurons of awake, normally-behaving mice. In contrast to low resolution BOLD-fMRI, MEMRI lends itself to study activity patterns in the brains of small animals at high resolution. In addition to our previous auditory studies (Yu et al., 2005; Yu et al., 2007), MEMRI has also been applied to study odor induced activity in the olfactory bulb (Pautler et al., 1998; Chuang et al., 2006), to examine light adaptation in retinal neurons (Berkowitz et al., 2006), to map cocaine-induced neuronal activation (Lu et al., 2007), and to detect hypothalamic activity (Morita et al., 2002; Chaudhri et al., 2006; Kuo et al., 2006) and ischemia-induced excitotoxicity (Aoki et al., 2003). Furthermore, MEMRI has been validated by correlation with BOLD and CBF (cerebral blood flow) functional maps in the somatosensory cortex of rats (Duong et al., 2000). Taken together, these results indicate that MEMRI brain mapping is a powerful new tool for analyzing activity patterns in the brains of small animals.

Cortical activity patterns have been studied previously in the mouse brain by optical imaging techniques, using voltage- and

* Corresponding author. Skirball Institute of Biomolecular Medicine, New York University School of Medicine, 540 First Avenue, New York, NY 10016, USA. Fax: +1 212 263 8214.
E-mail address: turnbull@saturn.med.nyu.edu (D.H. Turnbull).
Available online on ScienceDirect (www.sciencedirect.com).

1053-8119/$ - see front matter © 2007 Published by Elsevier Inc.
doi:10.1016/j.neuroimage.2007.08.029

calcium-sensitive dyes and two-photon microscopy for increased penetration (Grinvald et al., 1986; Denk et al., 1995; Svoboda et al., 1997; Mrsic-Flogel et al., 2003). However, even with two-photon microscopy the depth of optical penetration is limited to several hundred microns, with the result that deep brain activity cannot be analyzed using optical imaging. We still lack knowledge of how sensory stimuli are represented in important subcortical brain nuclei, such as the inferior colliculus (IC), the auditory midbrain. Neuroimaging methods such as MEMRI could enable the study of activity induced in deep brain regions of awake mice.

In this study, we focused on the auditory midbrain of mice, examining the sensitivity and specificity of MEMRI to detect activity patterns after sound-stimulation with defined frequency and amplitude components. The basic circuitry encoding acoustic signals in the central auditory system has been studied extensively (Popper and Fay, 1992; Pollak et al., 2003). Neuronal recordings demonstrated that auditory neurons in the ascending auditory pathway respond to a limited range of frequencies, and are arranged tonoptically (Aitkin and Moore, 1975; Merzenich et al., 1975; Romand and Ehret, 1990). This tonotopic organization is most applicable for sound stimuli near threshold activation of auditory neurons (Phillips et al., 1994). However, it is not only the auditory neurons with threshold response that are activated during acoustic perception, but also neurons with different frequency sensitivity firing together to represent each perceived sound stimulus. Therefore, analysis of activity patterns resulting from supra-threshold acoustic stimulation can therefore provide critical new insights into auditory processing.

In this study, sound-evoked activity patterns were represented using statistical *p*-value maps derived from MEMRI images. The methods used to generate these maps were similar to the voxel-wise statistical methods currently used in BOLD fMRI. Gaussian filtering was implemented to minimize false positive (Type I) errors produced by multiple comparisons. The *p*-value threshold was chosen to restrict false positives while still preserving the biological meaningful results. We found that setting the *p*-value threshold at 0.05, in combination with Gaussian filtering, resulted in 40-kHz activity patterns located in the ventral IC, in excellent agreement with previous electrophysiological results (Romand and Ehret, 1990). The 3D p-maps showed that both the volume of the 40-kHz activity regions and the peak MEMRI signal enhancement increased in proportion to the stimulus amplitude. Our results clearly demonstrate that MEMRI statistical mapping provides a sensitive and high-resolution method for mapping activity in deep brain nuclei of mice.

Materials and methods

Animals

All mice used in these studies were maintained under protocols approved by the Institutional Animal Care and Use Committee of New York University School of Medicine. The procedure to prepare the mice for MEMRI was described previously (Yu et al., 2005). Briefly, ICR mice were injected intraperitoneally (IP) with 0.4 mmol/kg body weight of $MnCl_2$ in saline at postnatal day (P) 19 (P0 denotes the day of birth), exposed to 24-h of defined sound stimulation or quiet, and then anesthetized with isoflurane gas (1–1.5% in air) during MRI at P20. During sound exposure or quiet, mice were maintained under normal living conditions, with a 12-h light/12 h dark cycle and free access to food and water. Neither Mn administration nor sound stimulation induced abnormal behavior during the 24-h time period.

Acoustic environment and stimuli

To analyze sound-evoked MEMRI enhancement patterns, mice were exposed to a 40-kHz pure tone stimulus at three different calibrated amplitudes: 65, 77 and 89 dB peak sound pressure level (SPL). For each stimulus, the 40-kHz carrier frequency was amplitude modulated at 4 Hz with a modulation range of 90%. Amplitude modulation was implemented in an attempt to avoid habituation of the IC neurons to the repetitive stimuli (Yu et al., 2005). Acoustic waveforms were generated on a programmable Function/Arbitrary Waveform Generator (Model 33220A, Agilent), amplified with a high fidelity audio amplifier (AMP-4030, Xplore), and delivered through an audio speaker (XT25TG30, VIFA). The speaker was mounted inside an acoustic isolation chamber (Mac-1, Industrial Acoustics) lined with polyurethane anechoic wedge panels (Acoustics First). Mice were kept in standard mouse microisolator cages, placed within the acoustic chamber during the 24-h period of sound exposure or quiet (control). The amplitude and spectral characteristics of the sound stimuli, as well as the noise floor, were measured with a multichannel spectrum analyzer (Bruel & Kjaer 3550) using a quarter-inch free-field condenser microphone. The system was calibrated with a Model 4294 vibration reference source.

MRI data acquisition

MRI was performed on a micro-imaging system (SMIS) consisting of a 7-Tesla (T) horizontal magnet (Magnex Scientific) with actively shielded gradients (Magnex: 250-mT/m gradient strength; 200-μs rise time) and a 25-mm (inner diameter) quadrature Litz mouse head coil (Doty Scientific). The coil was incorporated into a custom holder with a tooth bar to immobilize the head and a nosecone for isoflurane gas delivery with an anesthesia machine (VMS Matrix). T1-weighted brain images were acquired with a 3D gradient echo pulse sequence (echo time, TE = 4 ms; repetition time, TR = 50 ms; flip angle = 65°), resulting in a volumetric image set covering the entire brain, with isotropic spatial resolution of 100-μm in a total imaging time of 110 min per mouse.

Image processing

3D volumetric MR image data were processed with Amira (v3.1 Mercury Computer Systems-TGS) using the following steps: 1) The whole brain of each mouse was first segmented using the propagating active contour filter to detect the boundary between the brain tissue and the skull; 2) Each 3D mouse brain was registered to a 3D brain template that was created by averaging 13 registered mouse brains. As a result, each brain was aligned in the same coordinate system as the template; 3) To reduce the signal intensity differences produced by MRI acquisition variability, the histograms of the 3D whole brain images were normalized using a program written in IDL. Without changing the profile or detailed structure of the histograms, we modulated each histogram by shifting the mean and scaling the width resulting in whole brain histograms with equal mean and standard deviation; 4) The IC was extracted from each mouse brain in Amira, using an 3D IC mask segmented from the whole brain template. It should be noted that only rigid transformation between images were applied during registration to minimize

any effects of computational manipulation on the final results. The variation of the whole brain size among individual mice at the same age was small enough that image analysis could be performed in those registered images with rigid transformations only.

Statistical mapping and image analysis

Mn accumulation during sound stimulation results in T1-weighted MRI signal enhancement in active regions of the central auditory system (Yu et al., 2005). Matlab code was developed to generate and display statistical maps of the sound-evoked MEMRI enhancement in the IC, the auditory midbrain (v7.1, MathWorks). Voxel-wise Student's *t*-tests (two-tailed) were performed between sound-stimulated and quiet control 3D IC images (Fig. 1). We also performed a voxel-wise one-way Analysis of Variance (ANOVA), comparing sound stimulated images at three different amplitudes (65, 77 and 89 dB, peak SPL). Analyses were based on data from 11 quiet control mice, 8 mice stimulated with 89-dB peak SPL, 8 mice with 77-dB peak SPL and 10 mice with 65-dB peak SPL. 3D statistical p-maps were reconstructed by assigning the resulting *p*-value from each voxel-wise *t*-test or ANOVA analysis to the corresponding voxel of the 3D IC image. For the *t*-test analysis, a variable *p*-value threshold (p_{th}) was used to characterize the statistically significant voxels, comparing each sound-stimulated group to the quiet control group. The significant voxels therefore provide a quantitative representation of the patterns of sound-evoked MEMRI enhancement in the IC. Gaussian filtering was used to remove the sparsely distributed and noncontiguous voxels. This filtering step smoothed the 3D p-map, by convolving the data with a $3\times3\times3$ Gaussian filter kernel. This 3D Gaussian filter effectively reduced the number of false positive voxels (Type I errors), which are more likely to be separated from the main contiguous region (Friston et al., 1991; Forman et al., 1995). For most applications, a conventional threshold ($p_{th}=0.05$) was used in combination with Gaussian filtering to quantify the sound-evoked IC activity patterns. The p-maps were displayed as color-coded 2D slices or as 3D volumetric surface contours. Surface constraint visualization was applied for display purposes only, for visualizing the resulting 3D surface contours within the IC template.

Signal intensity (SI) differences were calculated for each voxel within the active IC regions of sound stimulated (s) and quiet control (c) mice:

$$\Delta SI = \{(SI_s - SI_c)/SI_c\}\cdot 100\ [\text{in }\%] \quad (1)$$

The 3D active IC regions (defined by p_{th} and Gaussian filtering) were used as region-of-interests (ROIs) for further analyses. Color-coded maps of ΔSI were generated by voxel-wise application of Eq. (1) within each ROI. In addition, the mean SI was calculated within each ROI for each mouse, and statistical analysis was performed on these SI values, comparing the stimulated and control groups using Student's *t*-test. Finally, linear regression analysis was used to examine the relationship between the peak stimulus SPL and the differences in SI within the ROIs defining the active regions of the IC. In this case, the maximum SI was detected in the ROI for each control mouse, and the peak SI was defined as the average of those maximum values, SI_{PC}. For each stimulated mouse, the peak SI was detected in the appropriate amplitude-dependent ROI, SI_{PS}. Then the peak change in SI was taken as the percent difference between SI_{PS} and SI_{PC} for each mouse:

$$\Delta SI_P = \{(SI_{PS} - SI_{PC})/SI_{PC}\}\cdot 100\ [\text{in }\%] \quad (2)$$

The regression line, *r*-value and 95% confidence levels were computed from these data.

Results

Statistical mapping of 40-kHz activity patterns in the mouse IC

Previously, we demonstrated that 40 kHz pure-tone stimulation enhanced the ventral IC regions of MEMRI images (Yu et al., 2005), which was in excellent agreement with the tonotopic map established in mice by electrophysiology (Romand and Ehret, 1990). In this study, our goal was to develop an unbiased and

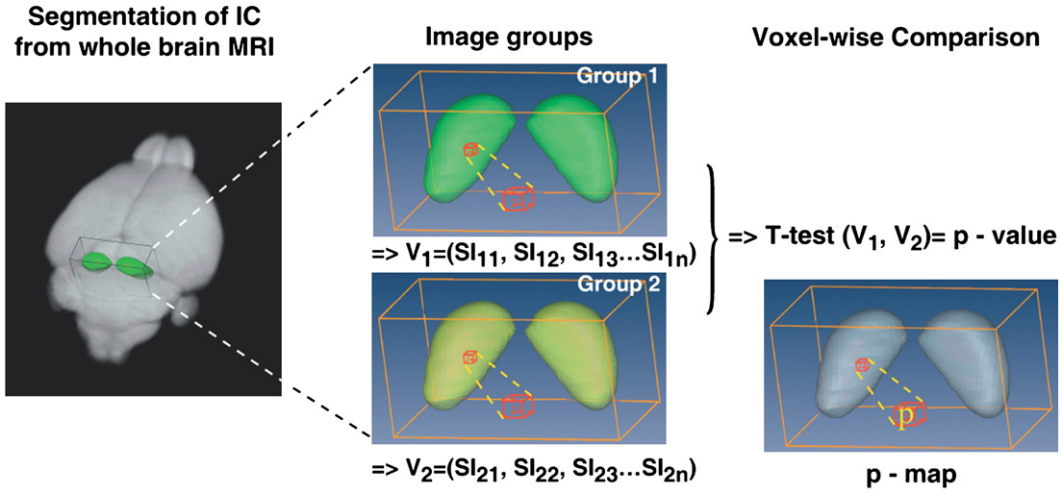

Fig. 1. Statistical mapping in the mouse IC from MEMRI images. 3D MEMRI images of the IC were segmented and analyzed via voxel-by-voxel statistical comparisons. *t*-test analysis was performed, comparing the signal intensities (SI) in each voxel, between 3D images from two groups of mice: V_1 array of SI values for Group 1=Stimulated; V_2 array for Group 2=Quiet controls. For each voxel (red cube), the resulting *p*-value was assigned after 8-bit gray scale conversion. In this way, a 3D p-map was created to encode the statistically significant different IC regions between the two groups of mice.

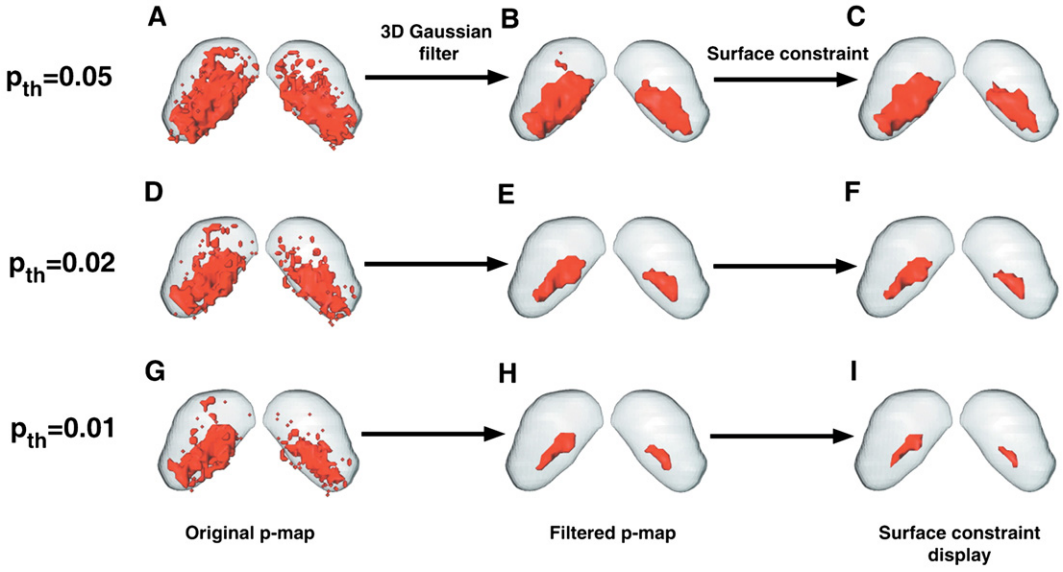

Fig. 2. Gaussian filtering is a method for reducing the number of false positive errors. Multiple voxel-wise t-tests were made, comparing MEMRI images of mice maintained in a quiet environment and mice exposed to 40 kHz. The resulting statistical maps demonstrated difference between the two groups (quiet vs. 40 kHz=red) using a variable *p*-value threshold (p_{th}): p_{th}=0.05 (A–C), p_{th}=0.02 (D–F), and p_{th}=0.01 (G–I). Some scattered active voxels were observed in the original statistical maps, which are more likely to be the false positive voxels (A, D, G). A 3D Gaussian filter was employed to smooth the 3D p-map by convolving the data with a 3×3×3 Gaussian kernel (B, E, H). A constrained smoothing function (Amira) was also employed for display purposes only, generating sub-voxel weights to naturally smooth the surface of the activity contour. In the example shown, this smoothing function has been applied to the filtered p-map data (C, F, I) to show the effect of the smoothing operation (Panel C reprinted with permission from Fig. 1H of Yu et al., 2007).

quantitative statistical mapping method to represent 3D sound-evoked MEMRI activity patterns in the mouse IC. Student's *t*-test was used for voxel-by-voxel comparisons of the IC signal intensities of stimulated (40-kHz, 89-dB peak SPL) and quiet control images (Fig. 1). The resulting *p*-value was assigned to the corresponding voxel to create a 3D p-map of the mouse IC.

Active IC voxels were defined as those with *p*-value below a specified threshold (p_{th}). To determine the effect of p_{th} on the results, p-maps were derived from MEMRI images with p_{th} ranging between 0.01 and 0.05 (Fig. 2). Threshold detection, in combination with Gaussian filtering, resulted in well-defined ventral IC contours for the 40-kHz activity pattern, in excellent agreement with the previous electrophysiological (Romand and Ehret, 1990) and MEMRI results (Yu et al., 2005). As expected, the volume of the active IC region was directly proportional to the magnitude of the *p*-value threshold, p_{th} (Fig. 2, Table 1). These results indicated that the statistical p-maps provided an unbiased and quantitative estimate of the region of sound-evoked activity, which can be used for comparing responses in mice after stimulation with different sound stimuli.

Table 1
Active voxel volume as a function of p_{th}

p_{th}	Pre-filtering	Post-filtering
0.05	1549	971
0.02	1007	301
0.01	735	129

The number of voxels was calculated before and after the Gaussian filtering step, demonstrating the reduction due to the removal of false positive voxels.

Sound amplitude-dependent MEMRI activity patterns in the mouse IC

To assess the relationship between sound amplitude and the distribution of sound-evoked activity, MEMRI images and p-maps were acquired from mice stimulated with 40 kHz pure-tones at three different amplitudes: Peak values of 65 dB, 77 dB, and 89 dB SPL (Fig. 3). The volume of the active IC increased in direct proportion to the amplitude of the stimulus (Figs. 3G–L; Table 2). These results indicated that increasing numbers of IC neurons, organized around a ventral region most sensitive to 40-kHz stimulation, were activated and accumulated Mn as the amplitude of the 40-kHz stimulus was increased.

Sound amplitude-dependent MEMRI signal intensities in the active IC

Further analyses were performed to investigate the relationship between sound amplitude and MEMRI signal enhancement (Fig. 4). Percent changes in signal intensity (ΔSI) were calculated using Eq. (1) for each voxel within the active IC regions defined by the statistical p-maps. The resulting intensity maps showed an increase in ΔSI with stimulus amplitude, with a peak value of approximately 20% at 89-dB SPL stimulation (Figs. 4A–C). The difference in mean SI, comparing stimulated and control mice, was close to 10%, independent the amplitude of the sound stimulus (Fig. 4D). These results indicate that although the active IC volume increased proportional to the stimulus amplitude, the average Mn accumulation and MEMRI signal enhancement over the active volume was relatively constant. Importantly, the mean SI measured in the 40-kHz stimulated mice was significantly

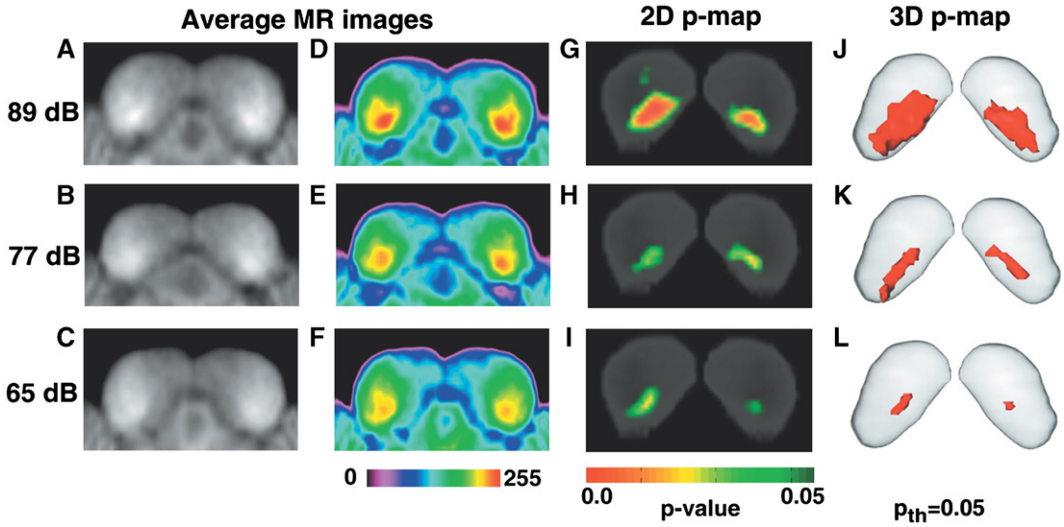

Fig. 3. MEMRI mapping revealed amplitude-dependent differences the distribution of 40-kHz IC activity. Increasing the peak sound pressure levels (SPL) of the 40-kHz stimulus induced increasing volumes of enhancement, comparing 65 dB, 77 dB, and 89 dB. Averaged coronal IC images ($n \geq 8$ in each group), displayed in grayscale (A, B, C) and pseudo-color coding (D, E, F; color bar below), demonstrated increasing signal intensity with increasing SPL. *t*-test comparison with the quiet control IC images resulted in p-maps, shown in 2D coronal sections (G, H, I; color bar below) and in 3D contours (J, K, L; *p*-value threshold, $p_{th}=0.05$ for each 3D map) (Panel G reprinted with permission from Fig. 2A of Yu et al., 2007).

higher than that in the quiet controls (Fig. 4D; $p<0.001$ for each amplitude).

In contrast to the mean SI, the peak changes in SI were observed to increase in proportion to stimulus amplitude. Quantitative analysis showed that the average peak percentage change in SI (ΔSI_P), computed using Eq. (2) was 7% for 65-dB SPL, 14% for 77-dB, and 20% for 89-dB. Linear regression analysis showed that ΔSI_P was directly proportional to the stimulus SPL (Fig. 4E), yielding a regression line given by the following equation:

$$\text{Predicted } \Delta SI_P = -0.3 + 0.00567 \cdot (\text{SPL in dB}) \quad (3)$$

Eq. (3) was observed to explain 59.7% of the variance in signal intensity (i.e., $r^2=0.597$, or $r=0.773$).

ANOVA analysis of amplitude-dependent IC activity

To obtain spatial information on the amplitude-dependent activity differences, we compared the 40-kHz stimulated images at three SPLs (65, 77 and 89 dB) using voxel-wise ANOVA analysis. The 3D ANOVA p-maps revealed regions of significant amplitude-dependent signal changes located primarily at the edge of the 89-dB active region (Fig. 5). This result suggested that the signal intensity differences noted above (Fig. 4) were largely due to activation of additional peripheral neurons by higher sound amplitudes, rather than by activity changes in the central 40-kHz region, which was responsive to all three SPLs.

Table 2
Active IC volume as a function of peak stimulus amplitude (SPL)

SPL	Active volume (# voxels)
89 dB	971
77 dB	247
65 dB	83

The number of voxels was calculated at different SPL, demonstrating the sound amplitude dependence of active IC volume.

Discussion

Our previous studies demonstrated that MEMRI provides a sensitive method to detect accumulated sound-evoked activity in the mouse IC (Yu et al., 2005, 2007). In this study, we developed and applied a statistical parametric mapping method for quantitative analysis of MEMRI activity patterns. We first analyzed the spatial distribution of activity patterns induced by 40-kHz pure tones at different sound amplitudes. The resulting statistical maps showed activity localized to the ventral IC regions, in excellent agreement with the tonotopic map established by electrophysiology. The volume of the active IC region increased in proportion to the amplitude of the 40-kHz stimulus. Analysis of the MEMRI data within the active regions demonstrated close to a 10% increase in average signal intensity, independent of sound amplitude, comparing stimulated to control mice. The peak signal intensity in the active IC regions was shown to increase in proportion to the stimulus amplitude, up to 20% at the highest sound amplitude. ANOVA analysis was used to identify and localize peripheral IC regions with significant amplitude-dependent signal intensity changes. Taken together, these results indicate that MEMRI can be used to analyze both the spatial location of neuronal activity in the mouse IC, as well as the magnitude of the activity evoked by sound stimuli carrying different energy.

One potential problem with the statistical mapping approach introduced in this study is that there is no standard method to minimize the number of false positive errors from multiple *t*-test comparisons, while preserving the biological meaning of the significant voxels. In particular, in statistical maps there is no method that can restrict false positive errors (Type I) without introducing false negative errors (Type II). Strategies have been developed to

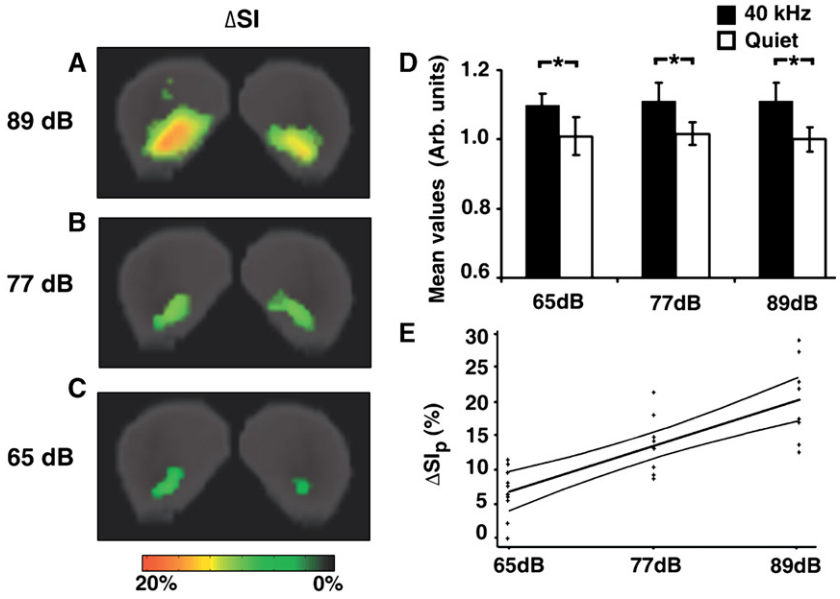

Fig. 4. MEMRI signal intensities were analyzed within the active IC regions defined by the 3D p-maps. Signal intensity (SI) differences (ΔSI) between sound stimulated and quiet control images were calculated in each voxel with p-value less than or equal to 0.05. Color-coded 2D maps show ΔSI in coronal sections of the IC (A, B, C; color bar below). (D) The mean SI was significantly higher in 40-kHz stimulated mice than in quiet controls (65-dB vs. Quiet, $p=0.00032$; 77-dB vs. Quiet, $p=0.00090$; 89-dB vs. Quiet, $p=0.00022$). (E) Scatter plot of the peak ΔSI versus peak sound stimulus amplitude, showing the regression line (center) and 95% confidence bands (outer curves).

reduce false positives, such as the Bonferroni correction, but these were too conservative to analyze sound evoked activity signals in this study. Specifically, there were no significant differences detected in sound stimulated images using the p-value threshold derived from Bonferroni correction (for 5245 voxels in the segmented mouse IC, $p_{th}=0.05/5245=0.0000095$; data not shown). As an alternative approach, we implemented Gaussian filtering to eliminate a significant number of false positive errors from the pre-filtering statistical image (Table 1). After Gaussian filtering, IC voxels with p-value less than 0.05 were consistently located in the ventral IC in mice stimulated with 40-kHz. These results are in good agreement with the known electrophysiological maps, and provide confidence that the defined significance threshold does enable detection of the biologically meaningful results. To further investigate this point, we also implemented the false discovery rate (FDR) method to estimate the number of false positives in the statistical parametric images after Gaussian filtering. Similar to the Bonferroni correction method, FDR was very conservative in estimating upper bounds on the number of false positive errors, but nevertheless produced results in general agreement with the Gaussian filtering approach (Supplementary Material).

Previous MEMRI studies have implemented statistical (t-test) mapping methods, based on analyses of difference images (post–pre Mn injection) acquired from individual animals. This is a logical approach for dynamic MEMRI studies, comparing signal differences over a single imaging session (Lu et al., 2007), or for MEMRI studies of Mn transport along axonal tracts after focal brain injection (Cross et al., 2004). These previous methods employed Z-statistical mapping, using random field theory to constrain the Type I error rate (Friston et al., 1990, 1991; Worsley et al., 1992), as opposed to our

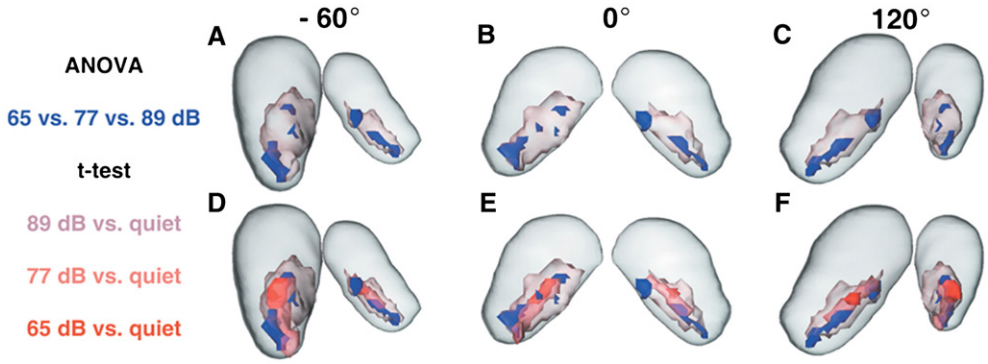

Fig. 5. One-way ANOVA analysis of sound stimulated images at different SPLs. Three coronally oriented views of the IC at different angles (−60°, 0°, and 120°) were displayed to visualize the 3D ANOVA p-map ($p_{th}=0.05$). IC regions with significant differences (blue) were located at the edge of the 89-dB active IC contour (pinkish-gray) within the IC anatomical template (gray) (A–C). The 3D ANOVA p-map was also superimposed on the composite map of all three t-test p-maps, further showing that the voxels with significant differences did not overlap with either the 65-dB (red) or 77-dB (pink) active IC contours defining the center of the 40-kHz activity pattern (D–F).

direct computation of *p*-value maps from *t*-statistics. In future, it would be interesting to investigate using a pre-stimulation MEMRI scan for auditory brain mapping, for normalizing subsequent post sound-stimulation images to the pre-scan. However, several issues would require careful examination, including the potential toxic effects of multiple Mn injections required for pre- and post-stimulation imaging. Moreover, the known developmental stage-dependent uptake of Mn in the mouse brain would likely preclude such an approach for studies of functional brain development (Wadghiri et al., 2004; Yu et al., 2007).

To properly analyze and interpret MEMRI activity patterns, it is necessary to understand the mechanistic basis of MRI signal enhancement related to neuronal activity. Previously, we showed that Mn ions accumulated in highly activated brain regions during prolonged periods of sensory stimulation, enabling assessment of accumulated activity patterns based on MEMRI signal enhancement (Yu et al., 2005). Two mechanisms are likely to serve as the bases for activity-induced Mn accumulation. First, repetitive sound stimulation leads to calcium channel activation, permitting the influx of extracellular Mn (Narita et al., 1990), which results in its accumulation within activated brain regions. Secondly, Mn can be transported along neuronal connections (Pautler, 2004). In our study, Mn ions could have entered auditory pathways close to the vasculature, including the organ of corti and cochlear nucleus (Yu et al., 2005). Since sound-evoked activity can also accelerate Mn trans-synaptic transport through neuronal projections (Van der Linden et al., 2004), the MEMRI signal enhancement patterns may represent both the accumulation due to sound-evoked synaptic activity and transport via the afferent projecting populations.

The excellent agreement between single tone MEMRI patterns and published isofrequency contour maps has further validated this approach for activity mapping (Fig. 3; Yu et al., 2007). Nonetheless, there are essential differences between the current MEMRI results and previous electrophysiological tonotopic maps. In MEMRI auditory brain mapping, a defined sound stimulus is used to evoke activity in a broad ensemble of neurons, while electrical recordings target one or a few auditory neurons to measure their response properties with a range of acoustic stimuli. To highlight the frequency selectivity of auditory neurons, isofrequency contour maps typically represent the spatial distribution of auditory neuron responses at threshold. However, within a population of neurons, the response threshold may vary by 20–40 dB (Romand and Ehret, 1990; Kiang et al., 1965; Tsuchitani, 1982). Thus, previous characterizations of tonotopy do not provide a full understanding of supra-threshold activity patterns.

In the current MEMRI study, we mapped the supra-threshold neuronal activity patterns of a single 40-kHz tone at different sound amplitudes. We showed that distinct neuronal ensembles within the 40-kHz isofrequency region were activated as sound pressure levels (SPL) increased. When the peak stimulus SPL was raised from 65 to 89 dB, the activated region expanded by 1.6 mm along the axis of the isofrequency contour, and by 0.55 mm across the contour width (i.e., dorsal–ventral) (Fig. 3). A similar expansion to supra-threshold tonal stimuli has been described previously in auditory cortex using optical mapping (Uno et al., 1993). These results highlight the fact that threshold tonotopic maps provide a good correlate to the main afferent projections, but do not reveal the functional representation that will emerge when the full range of projections and intrinsic connections are recruited.

In the current study, statistical (*t*-test) mapping from 3D MEMRI images demonstrated a direct relationship between sound amplitude and both the active IC volume (Table 2), as well as signal intensity changes (Fig. 4). Furthermore, MEMRI mapping revealed the 3D spatial patterns of IC neuronal ensembles activated by each test SPL (Fig. 3), as well as the distribution of IC neurons showing distinct firing properties to different SPLs (Fig. 5). To examine the exact relationship between MEMRI signal changes and SPL in the mouse midbrain, a number of factors need to be considered. In other mammals, the threshold levels in auditory neurons range over close to 40 dB SPL, and the dynamic ranges of the neuronal firing rate vs. sound level functions are variable (Kiang et al., 1965; Liberman, 1978; Aitkin, 1991). Some neurons in the auditory midbrain are known to have non-monotonic (not continuously increasing with sound level) firing characteristics (Ramachandran et al., 1999), but the spatial distribution and size of the non-monotonic population is currently unknown. Given this level of complexity, it is very difficult to predict the relationship between SPL and IC activity, and clearly more than three SPLs will be required to characterize the relationship between sound energy and MEMRI signal level and distribution.

In summary, the MEMRI statistical mapping approach introduced in this report provides an unbiased method to separate activity induced Mn accumulation in active brain regions from the nonspecific Mn distribution. The signal intensity changes between control and stimulated MEMRI images were analyzed quantitatively, and shown to provide a good representation of the activity patterns resulting from defined sound stimuli. We demonstrated the sensitivity of MEMRI mapping to detect and analyze sound frequency and amplitude dependent signal enhancement in the mouse IC. By altering the sound pressure levels, statistical mapping characterized the amplitude-dependent activity patterns induced by supra-threshold stimuli, providing the first insights into the organization of amplitude-dependent IC activity. Taken together, these results clearly indicate that MEMRI mapping provides a quantitative and unbiased method to assess activity in mice, enabling future analyses of the altered function in genetically and environmentally manipulated mouse models.

Acknowledgments

This research was supported by grants from the National Institutes of Health (NS038461, DC006892). We thank Dr. Youssef Zaim Wadghiri for advice on the MRI imaging protocols used in these studies. We thank the National Academy of Sciences for permission to reprint some data from our publication: Yu et al. (2007).

Appendix A. Supplementary data

Supplementary data associated with this article can be found, in the online version, at doi:10.1016/j.neuroimage.2007.08.029.

References

Aitkin, L., 1991. Rate-level functions of neurons in the inferior colliculus of cats measured with the use of free-field sound stimuli. J. Neurophysiol. 65, 383–392.

Aitkin, L.M., Moore, D.R., 1975. Inferior colliculus. II. Development of tuning characteristics and tonotopic organization in central nucleus of the neonatal cat. J. Neurophysiol. 38, 1208–1216.

Aoki, I., Ebisu, T., Tanaka, C., Katsuta, K., Fujikawa, A., Umeda, M.,

Fukunaga, M., Takegami, T., Shapiro, E.M., Naruse, S., 2003. Detection of the anoxic depolarization of focal ischemia using manganese-enhanced MRI. Magn. Reson. Med. 50, 7–12.

Bandettini, P.A., Wong, E.C., Hinks, R.S., Tikofsky, R.S., Hyde, J.S., 1992. Time course EPI of human brain function during task activation. Magn. Reson. Med. 25, 390–397.

Berkowitz, B.A., Roberts, R., Goebel, D.J., Luan, H., 2006. Noninvasive and simultaneous imaging of layer-specific retinal functional adaptation by manganese-enhanced MRI. Investig. Ophthalmol. Vis. Sci. 47, 2668–2674.

Chaudhri, O.B, Parkinson, J.R., Kuo, Y.T., Druce, M.R., Herlihy, A.H., Bell, J.D., Dhillo, W.S., Stanley, S.A., Ghatei, M.A., Bloom, S.R., 2006. Differential hypothalamic neuronal activation following peripheral injection of GLP-1 and oxyntomodulin in mice detected by manganese-enhanced magnetic resonance imaging. Biochem. Biophys. Res. Commun. 350, 298–306.

Chuang, K.H., Lee, J.H., Silva, A.C., Belluscio, L., Koretsky, A., 2006. Using manganese enhanced MRI to reveal active olfactory circuitry in response to odorant stimuli. Proc. 14th Annual Meeting of the ISMRM, New York, NY, p. 228.

Cross, D.J., Minoshima, S., Anzai, Y., Flexman, J.A., Keogh, B.P., Kim, Y., Maravilla, K.R., 2004. Statistical mapping of functional olfactory connections of the rat brain in vivo. NeuroImage 23, 1326–1335.

Denk, W., Piston, D.W., Webb, W.W., 1995. Two-photon molecular excitation in laser-scanning microscopy. In: Pawley, J.B. (Ed.), The Handbook of Biological Confocal Microscopy. Plenum Press, New York, NY, pp. 445–458.

Duong, T.Q., Silva, A.C., Lee, S.P., Kim, S.G., 2000. Functional MRI of calcium-dependent synaptic activity: cross correlation with CBF and BOLD measurements. Magn. Reson. Med. 43, 383–392.

Forman, S.D., Cohen, J.D., Fitzgerald, M., Eddy, W.F., Mintun, M.A., Noll, D.C., 1995. Improved assessment of significant activation in functional magnetic resonance imaging (fMRI): use of a cluster-size threshold. Magn. Reson. Med. 33, 636–647.

Friston, K.J., Frith, C.D., Liddle, P.F., Dolan, R.J., Lammertsma, A.A., Frackowiak, R.S., 1990. The relationship between global and local changes in PET scans. J. Cereb. Blood Flow Metab. 10, 458–466.

Friston, K.J., Frith, C.D., Liddle, P.F., Frackowiak, R.S.J., 1991. Comparing functional (PET) images: the assessment of significant change. J. Cereb. Blood Flow Metab. 11, 690–699.

Grinvald, A., Lieke, E., Frostig, R.D., Gilbert, C.D., Wiesel, T.N., 1986. Functional architecture of cortex revealed by optical imaging of intrinsic signals. Nature 324, 361–364.

Kiang, N.Y-S., Watanabe, T., Thomas, E.C., Clark, L.F., 1965. Discharge Patterns of Single Fibers in the Cat's Auditory Nerve. MIT Press, Cambridge, MA.

Kuo, Y.T., Herlihy, A.H., So, P.W., Bell, J.D., 2006. Manganese-enhanced magnetic resonance imaging (MEMRI) without compromise of the blood–brain barrier detects hypothalamic neuronal activity in vivo. NMR Biomed. 19, 1028–1034.

Liberman, M.C., 1978. Auditory-nerve response from cats raised in a low-noise chamber. J. Acoust. Soc. Am. 63, 442–455.

Lu, H., Xi, Z.X., Gitajn, L., Rea, W., Yang, Y., Stein, E.A., 2007. Cocaine-induced brain activation detected by dynamic manganese-enhanced magnetic resonance imaging (MEMRI). Proc. Natl. Acad. Sci. U. S. A. 104, 2489–2494.

Merzenich, M.M., Knight, P.L., Roth, G.L., 1975. Representation of cochlea within primary auditory cortex in the cat. J. Neurophysiol. 38, 231–249.

Morita, H., Ogino, T., Seo, Y., Fujiki, N., Tanaka, K., Takamata, A., Nakamura, S., Murakami, M., 2002. Detection of hypothalamic activation by manganese ion contrasted T(1)-weighted magnetic resonance imaging in rats. Neurosci. Lett. 326, 101–104.

Mrsic-Flogel, T., Hubener, M., Bonhoeffer, T., 2003. Brain mapping: new wave optical imaging. Curr. Biol. 13, 778–780.

Narita, K., Kawasaki, F., Kita, H., 1990. Mn and Mg influxes through Ca channels of motor nerve terminals are prevented by vermapil in frogs. Brain Res. 510, 289–295.

Ogawa, S., Lee, T.M., Kay, A.R., Tank, D.W., 1990. Brain magnetic resonance imaging with contrast dependent on blood oxygenation. Proc. Natl. Acad. Sci. U. S. A. 87, 9868–9872.

Ogawa, S., Menon, R.S., Tank, D.W., Kim, S.G., Merkle, H., Ellermann, J.M., Ugurbil, K., 1993. Functional brain mapping by blood oxygenation level-dependent contrast magnetic resonance imaging. A comparison of signal characteristics with a biophysical model. Biophys. J. 64, 803–812.

Pautler, R.G., 2004. In vivo, trans-synaptic tract-tracing utilizing manganese-enhanced magnetic resonance imaging (MEMRI). NMR Biomed. 17, 595–601.

Pautler, R.G., Silva, A.C., Koretsky, A.P., 1998. In vivo neuronal tract tracing using manganese-enhanced magnetic resonance imaging. Magn. Reson. Med. 40, 740–748.

Phillips, D.P., Semple, M.N., Calford, M.B., Kitzes, L.M., 1994. Level-dependent representation of stimulus frequency in cat primary auditory cortex. Exp. Brain Res. 102, 210–226.

Pollak, G.D., Burger, R.M., Klug, A., 2003. Dissecting the circuitry of the auditory system. Trends Neurosci. 26, 33–39.

Popper, A.N., Fay, R.R., 1992. The Mammalian Auditory Pathway: Neurophysiology (Springer Handbook of Auditory Research). Springer, New York, NY.

Ramachandran, R., Davis, K.A., May, B.J., 1999. Single-unit responses in the inferior colliculus of decerebrate cats. I. Classification based on frequency response maps. J. Neurophysiol. 82, 152–163.

Romand, R., Ehret, G., 1990. Development of tonotopy in the inferior colliculus. I. Electrophysiological mapping in house mice. Brain Res. Dev. Brain Res. 54, 221–234.

Svoboda, K., Denk, W., Kleinfeld, D., Tank, D.W., 1997. In vivo dendritic calcium dynamics in neocortical pyramidal neurons. Nature 385, 161–165.

Tsuchitani, C., 1982. Discharge patterns of cat lateral superior olivary units to ipsilateral tone-burst stimuli. J. Neurophysiol. 47, 479–500.

Uno, H., Murai, N., Fukunishi, K., 1993. The tonotopic representation in the auditory cortex of the guinea pig with optical recording. Neurosci. Lett. 150, 179–182.

Van der Linden, A., Van Meir, V., Tindemans, I., Verhoye, M., Balthazart, J., 2004. Applications of manganese-enhanced magnetic resonance imaging (MEMRI) to image brain plasticity in song birds. NMR Biomed. 17, 602–612.

Wadghiri, Y.Z., Blind, J.A., Duan, X., Moreno, C., Yu, X., Joyner, A.L., Turnbull, D.H., 2004. Mn-enhanced magnetic resonance imaging (MEMRI) of mouse brain development. NMR Biomed. 17, 613–619.

Worsley, K.J., Evans, A.C., Marrett, S., Neelin, P.A., 1992. Three-dimensional statistical analysis for CBF activation studies in human brain. J. Cereb. Blood Flow Metab. 12, 900–918.

Yu, X., Wadghiri, Y.Z., Sanes, D.H., Turnbull, D.H., 2005. In vivo auditory brain mapping in mice with Mn-enhanced MRI. Nat. Neurosci. 8, 961–968.

Yu, X., Sanes, D.H., Aristizabal, O., Wadghiri, Y.Z., Turnbull, D.H., 2007. Large-scale reorganization of the tonotopic map in mouse auditory midbrain revealed by MRI. Proc. Natl. Acad. Sci. U. S. A. 104, 12193–12198.